

Sinterability of nanopowders of terbia solid solutions with scandia, yttria, and lutetia

Stanislav S. BALABANOV^{a,*}, Dmitry A. PERMIN^a, Elena Ye. ROSTOKINA^a,
Sergey V. EGOROV^b, Andrey A. SOROKIN^b

^a*G.G. Devyatikh Institute of Chemistry of High-Purity Substances RAS, Nizhny Novgorod, Russia*

^b*Federal Research Center, the Institute of Applied Physics RAS, Nizhny Novgorod, Russia*

Received: February 8, 2018; Revised: June 7, 2018; Accepted: June 19, 2018

© The Author(s) 2018. This article is published with open access at Springerlink.com

Abstract: The synthesis of nanopowders of terbia compounds with scandia, yttria, and lutetia was carried out using a self-propagating high-temperature synthesis method involving a mixture of nitrates of metals and glycine as a precursor. The nanopowder phase transformations were investigated using X-ray diffraction analysis. It was found that lutetia has a negligible effect on the phase formation in terbia. On the other hand, yttrium and scandium ions significantly suppressed crystallization. The densification kinetics of nanopowders of the Tb_2O_3 compounds and the microstructure of ceramics after microwave sintering were studied using dilatometry and scanning electron microscopy. The introduction of scandia, yttria, or lutetia contributed to the intensification of the densification of the terbia ceramics when heated in a microwave field. Near full-density materials of terbia solid solutions with lutetia and yttria were obtained at about 1600–1640 °C. The ceramics of scandia–terbia compounds contained the second phase, which causes light scattering.

Keywords: terbia; microwave sintering; X-ray analysis; ceramics

1 Introduction

The fabrication of new crystalline materials for extreme light fields is one of the priorities of the science of advanced laser materials. One of the most urgent tasks in this field is the search for new Faraday isolator (FI) media. Such media should possess a high magnetic figure of merit and high thermal conductivity, low absorption and scattering coefficients at working wavelengths, and be potentially available for manufacturing with apertures of tens and hundreds of millimeters (to reduce the power density of radiation and any nonlinear effects

that might arise). The most common magneto-optical material used in modern FI in the wavelength range of 400–1100 nm is terbium–gallium garnet $Tb_3Ga_5O_{12}$ (TGG) single crystal. This is due to its relatively high values of the Verdet constant, high thermal conductivity, and low absorption coefficient ($< 0.1 \text{ cm}^{-1}$ at 1064 nm) [1]. However, the possibility of increasing the efficiency of magneto-optical media based on TGG single crystal is limited by the dimensions of the grown single crystal. Ceramic approaches developed over the past two decades in terms of obtaining highly transparent laser materials, have revealed the possibilities of creating new media with dimensions sufficient for use in high-power laser sources. A transparent TGG ceramic was first fabricated by Dr. Ikesue in 2002, and the possibility

* Corresponding author.

E-mail: Balabanov@ihps.nnov.ru

of its use in a high-power FI was reported in 2003 [2]. Further experiments confirmed the possibility of replacing the single crystal material with ceramics without a loss of functionality. In recent years some works have been published on the production of magneto-optical ceramics based on terbium–aluminum garnet $Tb_3Al_5O_{12}$ (TAG) [3,4] and terbium scandium aluminum garnet crystals (TSAG) [5,6], possessing a higher Verdet constant value and better thermo-optical properties in comparison with TGG. However, the use of these materials is limited by the maximum possible concentration of terbium in the structural unit (37.5 at%), which determines the Verdet constant.

In Ref. [7], it is reported that Tb_2O_3 ceramics with a Verdet constant more than three times higher than that for the TGG material within the 380–1750 nm transparency range, can be produced. Nevertheless, the ceramic samples used were not of laser quality. Tb_2O_3 ceramics technology is complicated by a number of issues. One of them is the mixed-valence state of terbium ions. There are several binary terbium oxides containing both Tb^{3+} and Tb^{4+} ions of various compositions TbO_x ($1.5 < x \leq 2$). At that Tb_2O_3 is easily oxidated at intermediate temperatures [8]. In the case of TbO_x powders sintering to Tb_2O_3 ceramics, oxygen gas is released inside the material during the sintering process ($TbO_x \leftrightarrow TbO_{1.5} + yO_2$) and the ceramics finally crack and/or break into pieces. Moreover, terbium(III) oxide undergoes a series of polymorphic transformations at high temperatures (near 1600, 2160, and 2340 °C), which causes volumetric change in the material, and induces mechanical stress and cracking [9–11]. Apparently, the maximum sintering temperature of Tb_2O_3 ceramics is limited to about 1500–1550 °C without sintering aid. Therefore, one of the most important tasks of the Tb_2O_3 ceramics technology is the search for sintering aid, in that this can promote sintering at lower temperatures, and/or can prevent the phase transitions at sintering temperatures and/or suppress mechanical stress caused by these phase transitions.

Such aids (or components, due to their high concentration in ceramics) may be rare earth sesquioxides (REO) such as Y_2O_3 , Sc_2O_3 , or Lu_2O_3 . However, information on obtaining Tb_2O_3 optical ceramic materials with REO is very limited [12]. In Refs. [13,14], the production of terbia solid solutions with oxides of some rare earth elements was reported. In addition, their existence ranges are determined, and the

questions of phase relationships (phase formation) in the systems $YO_{1.5}-TbO_{1.5}$, $Lu_2O_3-Tb_2O_3-TiO_2$ are considered.

In the present study, we report on the obtained nanopowders of $ScO_{1.5}-TbO_{1.5}$, $YO_{1.5}-TbO_{1.5}$, and $LuO_{1.5}-TbO_{1.5}$ compounds and Tb_2O_3 by self-propagating high-temperature synthesis using a mixture of nitrates of metals and glycine as a precursor. In addition, we study of the effect of scandia, yttria, and lutetia concentrations on the phase composition and the densification kinetics of the obtained powders, as well as the possibility of producing ceramics from these powders.

2 Experimental

Terbium(III, IV) oxide powders (Tb_4O_7 , 99.99% purity), yttrium oxide powders (Y_2O_3 , 99.99%), scandium oxide powders (Sc_2O_3 , 99.99%), lutetium oxide powders (Lu_2O_3 , 99.99%), nitric acid (99.999%), hydrogen peroxide (30% high-purity grade solution), and glycine (aminoacetic acid, NH_2CH_2COOH , 99.9%) were used as the starting materials in the present work.

The synthesis of powders of terbia compounds with scandia, yttria, and lutetia was carried out using the self-propagating high-temperature synthesis (SHS) method involving a mixture of nitrates of metals and glycine as a precursor. Terbium nitrate $Tb(NO_3)_3$ was prepared by dissolving Tb_4O_7 powders in a mixture of nitric acid (2 N) and hydrogen peroxide according to the procedure, described in Ref. [9]. $Y(NO_3)_3$, $Sc(NO_3)_3$, and $Lu(NO_3)_3$ were obtained by dissolving the corresponding metal oxide in nitric acid (2 N). Glycine was then added to the mixture of nitrates of the corresponding metals in a molar ratio of 1 : 1. The resulting glycine–nitrate solution was divided into portions, put in a quartz flask, and placed in a resistance furnace which had been preheated to 450 °C. The heating of the precursor led to the initiation of redox reactions and the promotion of the SHS. The combustion process was accompanied by intense gas formation. At the end of the combustion process, solid foam consisting of nanodisperse oxide particles was formed. Powders of thirteen various compositions ($Y_{1-x}Tb_x)_2O_3$, $(Sc_{1-x}Tb_x)_2O_3$, $(Lu_{1-x}Tb_x)_2O_3$ ($x = 0, 0.3, 0.6, 0.9, 1$) were obtained. SHS terbia-containing powders had brown colors of different intensities (the lightest shade is characteristic for $(Sc_{1-x}Tb_x)_2O_3$ compounds) due to the oxidation of

terbium ions during combustion. Additionally, the reduction of SHS powders was carried out by their calcination under a vapor flow of isopropyl alcohol at 650 °C.

The sintering of the ceramics based on terbia solid solutions or compounds with scandia, yttria, and lutetia was carried out by heating in a microwave (MW) field. The SHS powders were uniaxially pressed under 100 MPa into disks with a diameter of 10 mm and a thickness of 1 mm. The sintering of the powder compacts was carried out using a gyrotron-based setup operating at a frequency of 24 GHz with a regulated microwave power of up to 6 kW. The samples were placed in a thermo-insulated unit made of radio-transparent and heat-resistant porous material based on Al₂O₃. Such a unit made it possible to reduce heat loss significantly and to enhance the uniformity of the temperature distribution in a sample during its microwave heating. The thermo-insulated sample was located in the middle part of the working chamber of the gyrotron setup (typical size of the chamber was $L \approx 50\lambda_{em}$, where $\lambda_{em} = 1.25$ cm is the electromagnetic wavelength). The sample temperature was measured by an unshielded B-type thermocouple (Pt30%Rh/Pt6%Rh), which touched the bottom surface of the sample. The microwave sintering of the powder compacts was carried out at a residual air pressure of no more than 0.5 Pa. The maximum sintering temperature varied from 1450 to 1650 °C, and the sintering time ranged from 15 to 210 min. After the completion of the calcination, the microwave power was switched off automatically, and the powders, located in the thermo-insulated unit, were initially cooled at a rate of about 90 K/min then free-cooled at a lower rate.

X-ray diffraction (XRD) analysis of the powders (Y_{1-x}Tb_x)₂O₃, (Sc_{1-x}Tb_x)₂O₃, (Lu_{1-x}Tb_x)₂O₃ ($x = 0, 0.3, 0.6, 0.9, 1$) was done using an Ultima IV (Rigaku, Japan) X-ray diffractometer (Cu K α radiation, $\lambda = 1.5406$ Å). XRD was carried out in a range of angles

$2\theta = 15^\circ\text{--}60^\circ$ with a step of 0.02°, and an accumulation time of 1 s. The study of the phase composition was performed just after obtaining the SHS powders and their reduction (in a resistance furnace under a vapor flow of isopropyl alcohol at 650 °C). The morphology of the powders, the ceramic microstructure, and the average grain size were studied using an analytical scanning electron microscope (SEM) JEOL-6390LA using the imaging of back-scattered and secondary electrons. The sample density was determined by hydrostatic weighing with an accuracy of 0.01 g/cm³. The theoretical density of the solid solutions was calculated by the additive method.

The densification kinetics of solid solution or compound compacts (Y_{1-x}Tb_x)₂O₃, (Sc_{1-x}Tb_x)₂O₃, (Lu_{1-x}Tb_x)₂O₃ ($x = 0, 0.3, 0.6, 0.9, 1$) was investigated using a NETZSCH DIL 402C dilatometer (Netzsch) at a heating rate of 5 K/min at temperatures of up to 1530 °C, and under high vacuum conditions.

3 Results and discussion

The resulting powders (Y_{1-x}Tb_x)₂O₃, (Sc_{1-x}Tb_x)₂O₃, (Lu_{1-x}Tb_x)₂O₃ ($x = 0.3, 0.6, 0.9, 1$) have a sponge-like structure typical of SHS with randomly distributed pores, formed as a result of the intense gas formation during the synthesis process, and consisting of primary particles of several tens of nanometers in size (Fig. 1).

Figure 2 shows the X-ray diffraction patterns of the as-synthesized and reduced (Y_{1-x}Tb_x)₂O₃, (Sc_{1-x}Tb_x)₂O₃, (Lu_{1-x}Tb_x)₂O₃ ($x = 0.3, 0.6, 0.9, 1$) nanopowders. For comparison, Fig. 2 consists of the X-ray diffraction patterns of pristine yttria, lutetia, and scandia SHS powders.

SHS powders of pristine terbia ($x = 1$) consist of a mixture of crystalline phases. The peaks' positions in accordance with the theoretical X-ray Bragg reflections are most characteristic for compositions of Tb₇O₁₂ and

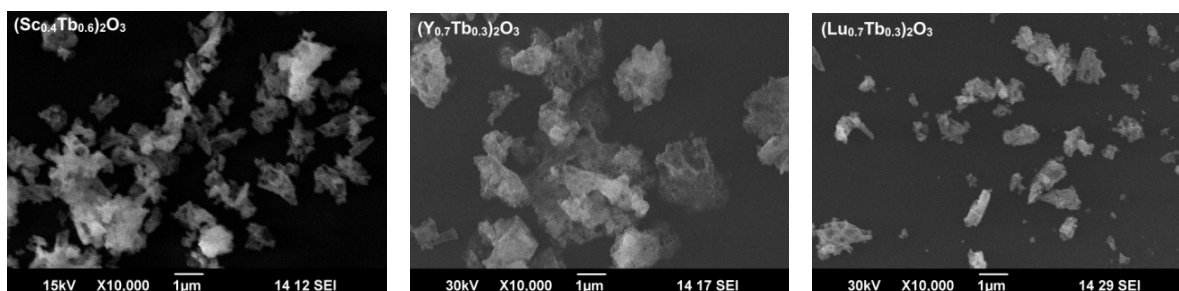


Fig. 1 SEM images of the powders of (Sc_{0.4}Tb_{0.6})₂O₃, (Y_{0.7}Tb_{0.3})₂O₃, and (Lu_{0.7}Tb_{0.3})₂O₃ after the SHS.

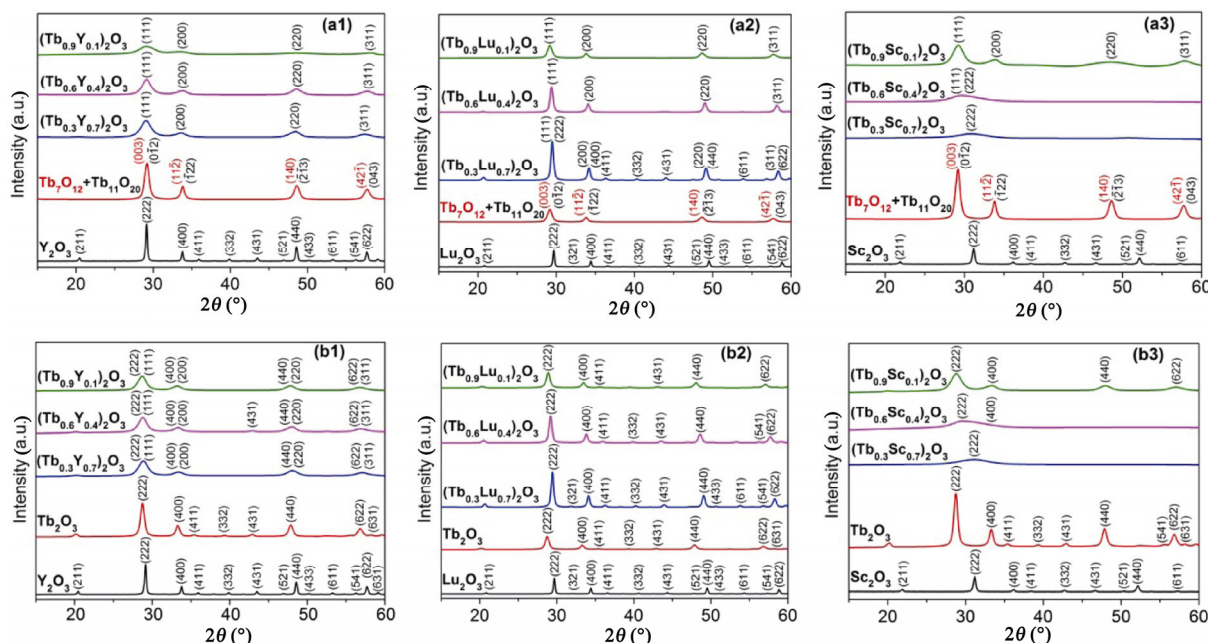


Fig. 2 XRD patterns of the powders (a1–a3) after the SHS and (b1–b3) after reducing in isopropyl alcohol vapor.

Tb₁₁O₂₀ intermediate phases [15]. The observed peaks are broadened due to low crystallite sizes and low crystallinity. Annealing of the SHS powders in a vapor flow of isopropyl alcohol at 650 °C leads to the reduction of terbium ions to the trivalent state. All diffraction peaks can be readily assigned to a pure cubic phase of Tb₂O₃ (the space group *Ia* $\bar{3}$) according to ICDD No. 00-023-1418 with a unit cell dimension of 10.730 Å.

In (Y_{1-x}Tb_x)₂O₃ (*x* = 0.3, 0.6, 0.9) terbia–yttria SHS powders (Fig. 2(a1)), there is a solid solution of cubic Y₂O₃ and triclinic Tb₁₁O₂₀ + trigonal Tb₇O₁₂ for all the compositions under consideration. The peaks’ positions for all three samples are almost the same, which is explained by the great similarity of the yttria and terbia XRD patterns, and by the significant peak broadening.

An appreciable amount of cubic Tb₂O₃ (10.7290 Å) appears in reduced powders of the same composition (Fig. 2(b1)). This manifests itself in a general shift of the peaks to the left and the appearance of a peak in the region of ~20°, which is not typical for other phases. The presence of cubic Tb₂O₃ is less obvious in powders with an yttrium content of 70 mol% (Y_{0.7}Tb_{0.3})₂O₃.

In the SHS powders of the terbia–lutetia (Lu_{1-x}Tb_x)₂O₃ system (*x* = 0.3, 0.6, 0.9) (Fig. 2(a2)), the peaks shift to the region of smaller diffraction angles (since the interplanar distance of Tb₂O₃ is greater) and the peaks’ intensity decreases as the Lu₂O₃ content in the mixture

diminishes. Samples with a lutetium content of 40 and 70 mol% represent the solid solutions of cubic Lu₂O₃ and mixtures of triclinic Tb₁₁O₂₀ and trigonal Tb₇O₁₂ terbium oxides. The XRD patterns of the sample with a lutetium content of 10 mol% is identical to that of 100% terbium oxide, i.e., a mixture of Tb₁₁O₂₀ + Tb₇O₁₂ phases.

In the reduced (Lu_{1-x}Tb_x)₂O₃ powders (Fig. 2(b2)), the existence of a solid solution of cubic lutetia and terbia with the same type of lattice symmetry is observed for all three dopant concentrations.

A different feature is observed in the terbia–scandia system (Sc_{1-x}Tb_x)₂O₃ (*x* = 0.3, 0.6, 0.9) (Fig. 2(a3)). At a scandia content of 40 and 70 mol%, a broad peak is observed in the 30° angle region, corresponding to the scandia maximum peak, which is substantially amorphized. At a scandia content of 40 mol%, the broad peak observed is somewhat shifted to the left, towards the terbium oxide peak position, which probably indicates a mixture of oxides. The XRD pattern of the sample with a scandia content of 10 mol% is almost identical to that of the 100% terbium oxides Tb₁₁O₂₀ + Tb₇O₁₂.

The XRD patterns of reduced powders with a scandia content of 40 and 70 mol% (Fig. 2(b3)) differ very little from those of unreduced powders of the same composition. At a scandia content of 10 mol%, the peak position is somewhat shifted to the left. A slight peak appears in the 20° angle region, which may

indicate the onset of a phase transformation of triclinic $Tb_{11}O_{20}$ and trigonal Tb_7O_{12} into a cubic structure.

The sizes of coherent-scattering regions calculated using the Scherrer's equation are presented in Table 1. It can be seen that the sizes of the coherent-scattering regions are 3–10 times smaller in scandia- and yttria-containing powders than in the lutetia-containing ones. Thus, yttrium and scandium ions substantially suppress the crystallization of the Tb_2O_3 powders, despite the fact that the Y^{3+} has an ionic radius closer to Tb^{3+} than the Sc^{3+} and Lu^{3+} ions.

Figure 3 shows the results of the dilatometric analysis of compounds of terbia with scandia, yttria, and lutetia ($x = 0.3, 0.6, 0.9$) powder compacts, and individual oxides ($x = 0, 1$). The densification of the pristine terbia sample ($x = 1$) begins at $567\text{ }^\circ\text{C}$, and the compact exhibits a total shrinkage of about 29% at $1520\text{ }^\circ\text{C}$. An intensive change in the shrinkage rate of the sample begins at $699\text{ }^\circ\text{C}$ and ends at $955\text{ }^\circ\text{C}$. In this temperature range, the reduction of the Tb^{4+} ions takes place. These ions have significant solubility in cubic Tb_2O_3 (up to 10% [9]) and can remain due to the incomplete reduction of the powder in alcohol vapor. Also, at these temperatures, an intense crystallization of powders occurs (SHS terbia powders, as well as scandia, yttria, and lutetia, have a low crystallinity after synthesis). This process can provide the system with an additional driving force leading to densification. It is known that a lattice transformation can activate the process of dislocation diffusion, resulting in the effective densification of ceramics [16]. After the reduction of TbO_x , the linear shrinkage of the sample continues up to a temperature of $1370\text{ }^\circ\text{C}$, after which the shrinkage rate begins to decrease.

A similar behavior is observed with regard to the Tb_2O_3 – Lu_2O_3 system. The introduction of 10 mol% of lutetia has a very limited effect on the densification rate of the samples compared with pristine terbia in the temperature range up to 1000 – $1100\text{ }^\circ\text{C}$, but the shrinkage

Table 1 Sizes of coherent-scattering regions of $(Y_{1-x}Tb_x)_2O_3$, $(Sc_{1-x}Tb_x)_2O_3$, $(Lu_{1-x}Tb_x)_2O_3$ powders (Unit: \AA)

x	$(Sc_{1-x}Tb_x)_2O_3$	$(Y_{1-x}Tb_x)_2O_3$	$(Lu_{1-x}Tb_x)_2O_3$
0.3	20.8(4)	53.9(5)	231.8(15)
0.6	19.7(4)	62.5(6)	194.6(9)
0.9	52.9(15)	38.7(7)	152.3(12)

rate increases with increasing temperature, which is characterized by a wide halo at temperatures above $1000\text{ }^\circ\text{C}$. The $(Lu_{0.1}Tb_{0.9})_2O_3$ compact exhibits a total shrinkage of about 33% at $1520\text{ }^\circ\text{C}$. An increase in the lutetia content in the samples to 40 and 70 mol% leads to an increase in the starting densification temperature (~ 730 – $740\text{ }^\circ\text{C}$) and a decrease in the shrinkage rate, which is especially characteristic of the $(Lu_{0.7}Tb_{0.3})_2O_3$ composition. The position of the first shrinkage peak maximum, corresponding to the reduction of the Tb^{4+} ions, shifts towards higher temperatures, while the peak intensity decreases. Also a tiny peak arises at $\sim 980\text{ }^\circ\text{C}$, characteristic of the crystallization of pristine lutetia. $(Lu_{0.4}Tb_{0.6})_2O_3$ and $(Lu_{0.7}Tb_{0.3})_2O_3$ compacts exhibit a total shrinkage of about 31% and 26% at $1520\text{ }^\circ\text{C}$, respectively. The lower shrinkage rate of compacts with high lutetia content $(Lu_{0.7}Tb_{0.3})_2O_3$ is likely caused by the higher sintering temperatures of pristine lutetia compared to terbia and an accelerating of this effect at its higher concentration in the sample.

A different situation is observed when terbia is doped by 10 mol% of yttria. The additive promotes an increase in the shrinkage rate of the compact in the entire studied temperature range. The compact $(Y_{0.1}Tb_{0.9})_2O_3$ exhibits a total shrinkage of about 35% at $1520\text{ }^\circ\text{C}$. An intensive change in the shrinkage rate of the sample begins at about $650\text{ }^\circ\text{C}$, which is lower than the temperature for pristine terbia, and ends at about $1000\text{ }^\circ\text{C}$. The introduction of even small amounts of yttria contributes to the intensification of terbia reduction (which agrees with the XRD data) and, as a consequence, to ceramic

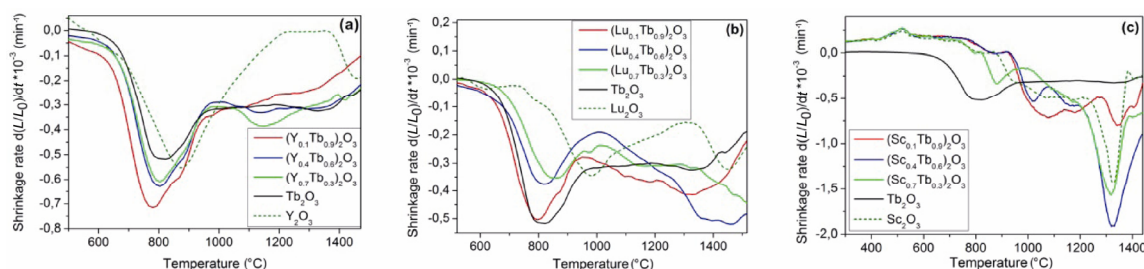


Fig. 3 Shrinkage rate curves of SHS powder compacts of terbia and compounds of terbia with (a) yttria, (b) lutetia, and (c) scandia.

densification. However, further dilution of the terbia matrix leads to a decrease in the shrinkage rate. For the $(Y_{0.1}Tb_{0.9})_2O_3$ and $(Y_{0.4}Tb_{0.6})_2O_3$ compositions, there is a peak that arises at ~ 870 °C, characteristic for the crystallization of pristine yttria. On the contrary, no such peak is found for the $(Y_{0.7}Tb_{0.3})_2O_3$ composition. A possible explanation for this may be that partial oxidation of Tb^{3+} results in distinct structural distortions of C-type solid-solutions with a terbium content of more than 50 mol% [13]. During reduction of terbium ions, two-phase system may appear [13] whose behavior is manifested on the dilatometric curves as a superposition of pristine yttria and terbia–yttria solid solution at temperatures below ~ 1000 °C. If terbium content is less than 50 mol% (for $(Y_{0.7}Tb_{0.3})_2O_3$ composition), the two-phase system does not appear, so a peak at ~ 870 °C is not observed. The densification rates of $(Y_{0.4}Tb_{0.6})_2O_3$ and $(Y_{0.7}Tb_{0.3})_2O_3$ samples have an intermediate value between pristine terbia and that doped by 10 mol% of yttria. The total shrinkage of $(Y_{0.4}Tb_{0.6})_2O_3$ and $(Y_{0.7}Tb_{0.3})_2O_3$ samples amounts to about 33% at 1520 °C.

The introduction of scandia into terbia leads to a significant decrease in the shrinkage rate of the samples in the temperature range up to 950 °C. This is associated with the lower content of tetravalent terbium ions in the samples. The lower content of Tb^{4+} is also noticeable in terms of the color of the reduced powders of the compounds $(Sc_{1-x}Tb_x)_2O_3$, which do not have a brown shade typical of $(Y_{1-x}Tb_x)_2O_3$ and $(Lu_{1-x}Tb_x)_2O_3$. Probably, scandia contributes to a slowing down of the process of terbium oxidation at the synthesis stage, the intensification of Tb^{4+} ions reduction, as well as the suppression of the crystallization of terbia–scandia compounds. On the dilatometric curves of terbia samples containing 40 and 70 mol% of scandia, only small peaks with a maxima at temperatures of about 1020 and 880 °C, respectively, are observed, which is probably responsible for the Tb^{4+} ion reduction. On the dilatometric curve of a terbia sample with 10 mol% of scandia, the shrinkage peaks are combined into one broad double peak. The

densification rate of the $(Sc_{0.1}Tb_{0.9})_2O_3$ sample at a temperature above 950 °C is higher than that of pristine terbia. At temperatures above 1100 °C, a significant increase in the shrinkage rate is observed in $(Sc_{0.4}Tb_{0.6})_2O_3$ and $(Sc_{0.7}Tb_{0.3})_2O_3$ samples, which is shown by a very intense peak on the dilatometric curves. The position of the peaks' maxima almost coincides with the position of the corresponding peak for pristine scandia, but the densification rate (compared to Sc_2O_3) is much higher. The effect of the increasing densification rate of the terbia–scandia compounds at high temperatures can be explained by activation of the dislocations diffusion due to the formation of terbium scandiate $TbScO_3$ (as will be seen later).

The estimation of the sinterability of SHS powders of compounds of terbia with scandia, yttria, and lutetia microwave sintering was carried out in the temperature range of 1450–1720 °C for 15–210 min. The prospects of using MW heating for production of optical ceramics are determined by the following main factors. The absence of heating elements in the working chambers ensures sintering in high vacuum conditions. Pollution of grain boundaries with the material of the evaporating heating elements is a significant issue in the process of ceramic sintering in the traditional ovens. Due to the volume character of MW heating, the temperature distribution has a maximum inside the sintered product, by contrast with the temperature distribution in the case of resistive heating. At this temperature profile, porosity on the product periphery remains open until a later sintering stage, which contributes to ejection of pores and achievement of a higher compaction rate. Figure 4 shows some SEM micrographs of the MW sintered samples. The density of the samples after sintering and the estimated values of the average grain size, are shown in Table 2.

As can be seen from Fig. 4 and Table 2, the introduction of yttria, lutetia, and scandia to terbia leads to an increase, both in the ceramic density and in the average grain size (which is typical for mixed

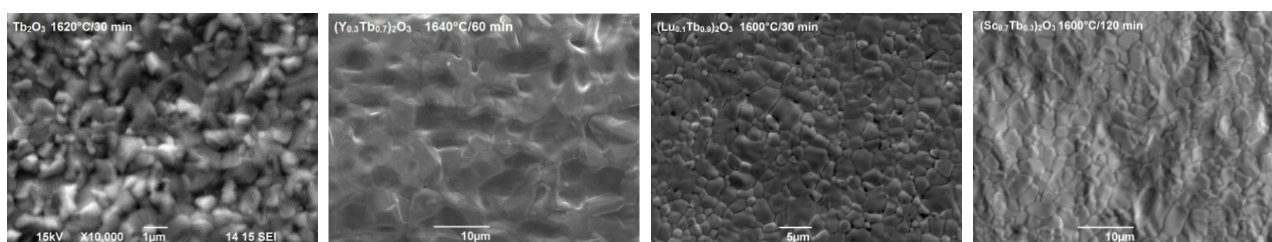


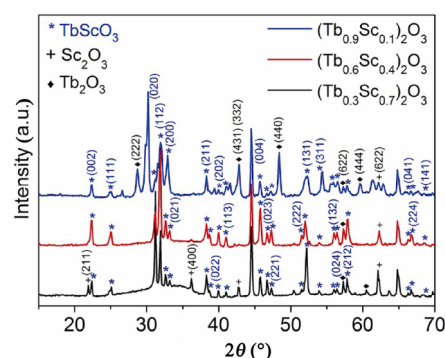
Fig. 4 SEM micrographs of Tb_2O_3 , $(Y_{1-x}Tb_x)_2O_3$, $(Lu_{1-x}Tb_x)_2O_3$, and $(Sc_{1-x}Tb_x)_2O_3$ microwave sintered ceramics.

Table 2 Density and average grain size of the samples after microwave sintering

Sample	Sintering temperature (°C)	Soaking time (min)	Density ρ (g/cm ³) and $\rho/\rho_{\text{theoretical}}$	Grain size (μm)
Tb ₂ O ₃	1450	15	6.475, 0.82	<0.2
Tb ₂ O ₃	1620	30	7.372, 0.93	1
(Y _{0.3} Tb _{0.7}) ₂ O ₃	1640	60	6.61, 0.95	6
(Y _{0.9} Tb _{0.1}) ₂ O ₃	1640	60	5.29, 0.99	7
(Lu _{0.7} Tb _{0.3}) ₂ O ₃	1500	60	6.67, 0.75	1.5
(Lu _{0.7} Tb _{0.3}) ₂ O ₃	1650	60	8.7, 0.972	4
(Lu _{0.4} Tb _{0.6}) ₂ O ₃	1600	30	8.394, 0.989	1.5
(Lu _{0.4} Tb _{0.6}) ₂ O ₃	1600	210	8.395, 0.99	4
(Lu _{0.4} Tb _{0.6}) ₂ O ₃	1650	60	8.37, 0.986	3
(Lu _{0.1} Tb _{0.9}) ₂ O ₃	1600	30	7.957 (0.99)	3
(Lu _{0.1} Tb _{0.9}) ₂ O ₃	1600	210	7.96 (0.99)	4
(Lu _{0.1} Tb _{0.9}) ₂ O ₃	1640	30	7.807 (0.971)	5
(Sc _{0.7} Tb _{0.3}) ₂ O ₃	1600	120	4.693 (0.961)	4
(Sc _{0.4} Tb _{0.6}) ₂ O ₃	1600	100	6.007 (0.972)	1.5
(Sc _{0.1} Tb _{0.9}) ₂ O ₃	1600	100	5.75 (0.769)	2.5

oxides of other rare earth metals) at identical sintering temperatures. The obtained data are in good agreement with the results of dilatometric analysis, which indicates an increase in the densification of mixed oxides compared with pristine terbia. Thus, the sintering of terbia samples with 10 and 40 mol% of lutetia at a temperature of 1600 °C for 30 min leads to the producing of ceramics with density equal to 99% of theoretical value. (Lu_{0.4}Tb_{0.6})₂O₃ and (Lu_{0.1}Tb_{0.9})₂O₃ samples are characterized by grain size distribution with maxima at about 1.5 and 3 μm respectively. A further increase in temperature or sintering time leads to an increase in the average grain size. The ceramic samples of terbia with 70 mol% of lutetia at the same sintering temperatures have quite a few pores at the grain boundaries, which form cavities comparable in size or larger than grains. This might be caused by the higher sintering temperatures of lutetia (compared with terbia) and the enhancement of this effect with an increase in its content in the sample. Consequently, each composition requires the selection of its own sintering conditions. The addition of more than 10 mol% of scandia to terbia contributes to the intensification of the sintering of the samples in comparison with pristine Tb₂O₃. However, the densification rate and the density values at identical sintering temperatures are somewhat lower than those for solid solutions with yttria and lutetia. This can be explained by the presence of the mixture of oxides Sc₂O₃, TbScO₃, Tb₂O₃ in the (Sc_{1-x}Tb_x)₂O₃ sintered ceramics (see Fig. 5). Also, a diffuse halo corresponding to the amorphous state is observed in the region of the most intense peak in the XRD patterns of (Sc_{1-x}Tb_x)₂O₃ sintered ceramics.

Nevertheless, despite the high density, all the samples

**Fig. 5** XRD patterns of (Sc_{1-x}Tb_x)₂O₃ ceramics.

are only translucent; the light transmission at a wavelength of 1 μm does not exceed 30% (see Fig. 6). The low transmission of terbia–yttria and terbia–lutetia solid solution ceramics is connected with the presence of inter- and intragranular pores, which are the main cause of light scattering. Their formation can be associated with both the non-optimal sintering mode of the samples, and the oxygen release that occurs during the reduction of the Tb⁴⁺ ions at temperatures of 700–1000 °C. The pressure of the oxygen trapped within a closed pore counteracts the surface tension driving force to shrink the pore during sintering. Further improvement in the optical quality of ceramics can be achieved by optimizing the sintering conditions.

In the case of compounds of terbia with scandia, the pore concentration is noticeably lower and insufficient for such intense scattering. In this connection, we assume that the main scattering mechanism in these samples is second phase scattering. This assumption can be confirmed by a significant (2%–3%) deviation in the ceramic density from the theoretical value against a background of insignificant porosity.

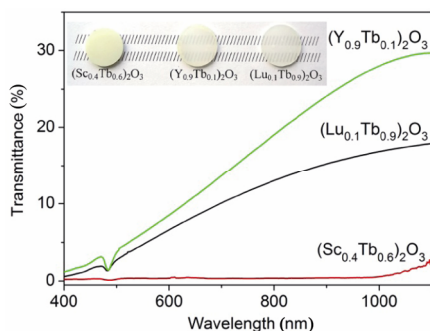


Fig. 6 Transmission spectrum and appearance of $(\text{Sc}_{0.4}\text{Tb}_{0.6})_2\text{O}_3$, $(\text{Y}_{0.9}\text{Tb}_{0.1})_2\text{O}_3$, and $(\text{Lu}_{0.1}\text{Tb}_{0.9})_2\text{O}_3$ ceramics.

4 Conclusions

Nanopowders of terbia compounds with scandia, yttria, and lutetia were successfully produced by the SHS method using a mixture of nitrates of metals and glycine as a precursor. The XRD patterns have indicated that the $(\text{Y}_{1-x}\text{Tb}_x)_2\text{O}_3$ and $(\text{Lu}_{1-x}\text{Tb}_x)_2\text{O}_3$ samples ($x = 0.3, 0.6, 0.9$) represent solid solutions of yttria or lutetia and terbia. A mechanical mixture of oxides Sc_2O_3 , TbScO_3 , Tb_2O_3 and amorphous phase is typical for the $(\text{Sc}_{1-x}\text{Tb}_x)_2\text{O}_3$ sample. Lutetium ions have a negligible effect on the phase formation in terbia; on the contrary, yttrium ions and, especially, scandium ions significantly suppress crystallization and formation of the Tb_2O_3 cubic phase.

The introduction of small amounts of yttria or lutetia contributes to the intensification of the terbia ceramics' densification and producing of samples with density equal to 99% of theoretical value when heated in a microwave field. The lower densification rate and the density of ceramics of compounds of scandia–terbia are due to the presence of the second phases. The study conducted on the temperature and composition dependences of the phase transformations and on the microstructure in polycrystalline terbia with the addition of yttria, lutetia, and scandia formed the basis for the development of new technology of high optical quality terbia-based ceramics for magneto-optical laser devices.

Acknowledgements

This work was supported by the Russian Foundation for Basic Research (Grant No. 16-03-00595).

References

- [1] Snetkov IL, Voitovich AV, Palashov OV, *et al.* Review of Faraday isolators for kilowatt average power lasers. *IEEE J Quantum Elect* 2014, **50**: 434–443.
- [2] Khazanov EA. Investigation of Faraday isolator and Faraday mirror designs for multi-kilowatt power lasers. In: Proceedings Volume 4968, Solid State Lasers XII. Scheps R, Ed. 2003: 115.
- [3] Chen C, Yi X, Zhang S, *et al.* Vacuum sintering of $\text{Tb}_3\text{Al}_5\text{O}_{12}$ transparent ceramics with combined TEOS+MgO sintering aids. *Ceram Int* 2015, **41**: 12823–12827.
- [4] Starobor A, Zheleznov D, Palashov O, *et al.* Study of the properties and prospects of Ce:TAG and TGG magneto-optical ceramics for optical isolators for lasers with high average power. *Opt Mater Express* 2014, **4**: 2127–2132.
- [5] Snetkov IL, Yasuhara R, Starobor AV, *et al.* Thermo-optical and magneto-optical characteristics of terbium scandium aluminum garnet crystals. *IEEE J Quantum Elect* 2015, **51**: 1–7.
- [6] Starobor A, Yasuhara R, Snetkov I, *et al.* TSAG-based cryogenic Faraday isolator. *Opt Mater* 2015, **47**: 112–117.
- [7] Snetkov IL, Permin DA., Balabanov SS, *et al.* Wavelength dependence of Verdet constant of $\text{Tb}^{3+}:\text{Y}_2\text{O}_3$ ceramics. *Appl Phys Lett* 2016, **108**: 161905.
- [8] Adachi G, Imanaka N. The binary rare earth oxides. *Chem Rev* 1998, **98**: 1479–1514.
- [9] Balabanov SS, Permin DA, Rostokina EY, *et al.* Synthesis and structural characterization of ultrafine terbium oxide powders. *Ceram Int* 2017, **43**: 16569–16574.
- [10] Zinkevich M. Thermodynamics of rare earth sesquioxides. *Prog Mater Sci* 2007, **52**: 597–647.
- [11] Coutures J, Rouanet A, Verges R, *et al.* Etude a haute température des systèmes formes par le sesquioxyde de lanthane et les sesquioxydes de lanthanides. I. Diagrammes de phases ($1400^\circ\text{C} < T < T$ Liquide). *J Solid State Chem* 1976, **17**: 171–182.
- [12] Shimada T. Magneto-optical ceramic material and method for selecting same. US Patent 9052415 B2. 2012.
- [13] Glushkova VB. Phase ratios in $\text{YO}_{1.5}\text{-TbO}_{1.5}$ and $\text{YO}_{1.5}\text{-TbO}_x$ systems. *Inorg Mater (USSR) (Engl Transl)* 1988, **24**: 665–669.
- [14] Petrova MA, Grebenshchikov RG. Specific features of the phase formation in the titanate systems $\text{Ln}_2\text{TiO}_5\text{-Ln}'_2\text{TiO}_5$ ($\text{Ln} = \text{La, Gd, Tb, Er; Ln}' = \text{Tb, Lu}$). *Glass Phys Chem* 2008, **34**: 603–607.
- [15] Zhang J, Von Dreele RB, Eyring L. The structures of Tb_7O_{12} and $\text{Tb}_{11}\text{O}_{20}$. *J Solid State Chem* 1993, **104**: 21–32.
- [16] Yavetskiy RP, Baumer VN, Danylenko MI, *et al.* Transformation-assisted consolidation of $\text{Y}_2\text{O}_3:\text{Eu}^{3+}$ nanospheres as a concept to optical nanograin ceramics. *Ceram Int* 2014, **40**: 3561–3569.

Open Access The articles published in this journal are distributed under the terms of the Creative Commons Attribution 4.0 International License (<http://creativecommons.org/licenses/by/4.0/>), which permits unrestricted use, distribution, and reproduction in any medium, provided you give appropriate credit to the original author(s) and the source, provide a link to the Creative Commons license, and indicate if changes were made.